Journal of Cellular Plastics

Fracture Toughness of High Density Polycarbonate Microcellular Foams

Martin N. Bureau and Vipin Kumar

The online version of this article can be found at:
http://cel.sagepub.com/cgi/content/abstract/42/3/229

Published by:

Additional services and information for *Journal of Cellular Plastics* can be found at:

Email Alerts: http://cel.sagepub.com/cgi/alerts

Subscriptions: http://cel.sagepub.com/subscriptions

Reprints: http://www.sagepub.com/journalsReprints.nav

Permissions: http://www.sagepub.com/journalsPermissions.nav

Fracture Toughness of High Density Polycarbonate Microcellular Foams*

MARTIN N. BUREAU[†]

Industrial Materials Institute, National Research Council Canada
75 de Mortagne Blvd., Boucherville, Québec, J4B 6Y4, Canada

VIPIN KUMAR

Department of Mechanical Engineering, University of Washington
Box 352600, Seattle, WA 98195, USA

ABSTRACT: Microcellular foams (MCFs) of polycarbonate (PC) with relative densities of 0.9 and 0.7 (MCF-0.9 and MCF-0.7) are produced by solid-state foaming. Microstructural characterization shows that they have bi-modal distribution of spherical cells, with median cell sizes of 3–4 µm and 6–9 µm for both cell populations. Tensile testing shows that ultimate tensile strength and Young's modulus approximately ranked with relative density, although MCF-0.9 has a modulus similar to the unfoamed PC (uPC). Toughness measurements show that, when compared to uPC on a critical stress intensity factor basis, MCF-0.9 shows no reduction in toughness and MCF-0.7 shows a ≈35% reduction. When compared to uPC on strain energy basis, 12–15% increases in toughness are measured for both MCFs. Their fracture occurs by multiple initiation, growth, and coalescence of voids formed at cells acting as stress concentrators. A fine cell morphology results in prolonged growth and coalescence phases, and thus improves fracture toughness.

KEY WORDS: microcellular foams, polycarbonate, mechanical properties, fracture toughness, crack propagation.

INTRODUCTION

Microcellular foams (MCFs) are foams with average cell size of the order of $10\,\mu m$ and below, very high cell nucleation density (e.g., $\approx 10^9$ cells/cm^3), and typical relative density of 0.5–0.7. MCFs were initially processed using a thermodynamic instability [1] to cause bubble nucleation and growth in the solid state. A two-stage approach was then developed [2], which involves gas saturation of a polymer at elevated pressure and room temperature, followed by a rapid pressure drop to atmospheric pressure, causing gas supersaturation, and heating to a temperature near the glass transition temperature to soften the polymer.

MCFs have attracted considerable attention because their mechanical properties, especially fracture-related, have been claimed to be similar to those of their unfoamed counterpart. This has been attributed to an 'inherently critical flaw size', below which cells do not act as defects. Evidence was brought in to support this behavior, namely, that impact strength is improved in the MCFs with respect to unfoamed polymers [3–5]. Significantly increased notched Charpy impact strength of polycarbonate (PC) MCFs [4] was reported for a relative density of 0.80 and an average cell size of $40\,\mu m$, but lower cell size of $10–20\,\mu m$ did not lead to such improvements. Notched Izod impact strength of PC MCFs with a relative density of 0.7 showed that it doubled when cell size changed from 7 to $18\,\mu m^3$. While these do show impact strength improvement with respect to their unfoamed version, increased impact strength at higher average cell size in the range of $18–40\,\mu m$ does not correspond to the definition of MCFs and is not in agreement with the flaw size upper limit. Moreover, several studies [3, 6–8] showed that the basic mechanical properties of MCFs, such as their Young's modulus or their tensile strength, are proportional to their density, in agreement with Gibson and Ashby [9], which is not in agreement with MCFs claimed behavior.

A number of reasons could explain these contradictory results. Charpy or Izod impact specimen preparation techniques, where different notch sharpness, type and importance of notch tip damage or micro-cracking, and local heating and melting at the notch root can be produced using high-speed cutting tools, can account for most of them. This is especially true in the presence of cells of different sizes in the notch vicinity. These phenomena are even more complex when MCFs based on different polymers are compared due to their different notch sensitivities. In addition, impact strengths reflect the combination of crack initiation, growth, and coalescence, which are not controlled in impact testing and

vary in intensity depending on the latter notch- or materials-related features. Moreover, these techniques are used to comment on fracture toughness, which is the measure of crack resistance to propagation, and not on initiation. Because of these reasons, comparison of the Charpy or Izod impact response is quite difficult and should be kept to quality control and materials specification, as stated by ASTM [10,11].

The objective of this study is to characterize the fracture toughness of PC MCFs with different densities, to understand their fracture behavior, and to provide a rationale comparison of MCF toughness to unfoamed polymers.

EXPERIMENTAL

All MCF specimens were prepared from 3 mm thick GE Lexan 9034 PC sheet cut into 75×75 mm plates. To produce the specimens with a nominal relative density of 0.7, plates were saturated in a pressure vessel kept at $22°$C at 4 MPa with carbon dioxide for a period of 10 days. The specimens were removed from the vessel and allowed to desorb gas for 5 min, then foamed in a hot water bath at $90°$C for 10 min followed by quenching in room temperature water to stop further bubble growth. For specimens with a relative density of 0.9, plates were saturated at $22°$C at 5 MPa for 14 days, and then foamed at $86°$C for 10 min followed by quenching in room temperature water.

The density of both MCFs was measured by Archimedes' method. The first MCF had a density of 1.073 g/cm^3 or 0.897 in relative density and was designated as MCF-0.9. The second had a density of 0.830 g/cm^3 or 0.694 in relative density and was designated as MCF-0.7. Their morphology was characterized by image analysis of scanning electron microscopy (SEM) observations of surfaces obtained cryogenic fracture. The through-thickness surfaces normal to the machine direction and to the transverse direction were characterized. Number-average cell size was calculated from the area of individual cells as equivalent diameter of a circle. A minimum count of 900 cells was employed for the determination of each cell size distribution.

The tensile tests were performed according to ASTM D638 on machined type IV dogbones with as-received thickness of 3 mm. The tests were carried out at 5 mm/min using a computer-controlled Instron mechanical tester and longitudinal and transverse extensometers. The load–displacement curves were monitored during these tests. Five specimens were tested for each material. Young's modulus (E), ultimate tensile strength (UTS), Poisson's ratio (ν) and strain at break (ε_b) were calculated.

Fracture toughness measurements were performed according to ASTM E1820 on machined compact-tension (CT) specimens with as-received thickness (B), width (W) of 50 mm, and notch depth of 11 mm. Precracking was made using a fresh razor blade introduced manually at the notch tip. The tests were carried out at 10 mm/min using a computer-controlled Instron servo-hydraulic tester and a clip-on crack opening displacement (COD) gage. The specimens were loaded until crack propagation was observed and then unloaded. Three specimens were tested for each material. Several loading/unloading cycles were made. After the final loading/unloading cycle, the specimens were completely fractured to measure the individual crack propagation using SEM. The load–COD curves were monitored during these tests. Critical stress intensity factor K_c, elastic fracture energy J_{el} at crack propagation onset, and total fracture energy during crack propagation J_{tot} were calculated according to ASTM E1820 using the following:

$$K_c = \frac{P_c}{B\sqrt{W}} f\left(\frac{a}{W}\right) \tag{1}$$

$$J_{el} = \frac{K_c^2 (1 - \nu^2)}{E} \tag{2}$$

$$J_{tot} = J_{el} + \frac{\eta A_{pl}}{B(W - a_o)} \tag{3}$$

where P_c is the critical load at crack propagation onset (determined from load at non-linearity), a and a_o are the instantaneous and initial crack lengths, f is a geometric function of normalized crack length, η is a constant equal to 2, and A_{pl} is the area under the load–COD curve for individual crack extension.

RESULTS

SEM observations of cryogenically fractured specimens were made. A typical skin/sub-skin/core morphology was observed for all MCFs specimens. Absence of cells characterized the skin layer, regular bi-modal type spherical cells were observed in core region and a transitory sub-skin region with quite large cells, and finer ones were observed between skin and core. The core represented 80% of the surface, and skins and sub-skins 10% each. Image analysis was carried out to obtain cell size distribution. The cell size distribution and cell morphology is shown in Figure 1. The MCF-0.9 had median cell sizes of 4 and 9 μm and MCF-0.7 had median cell sizes of 3 and 6 μm.
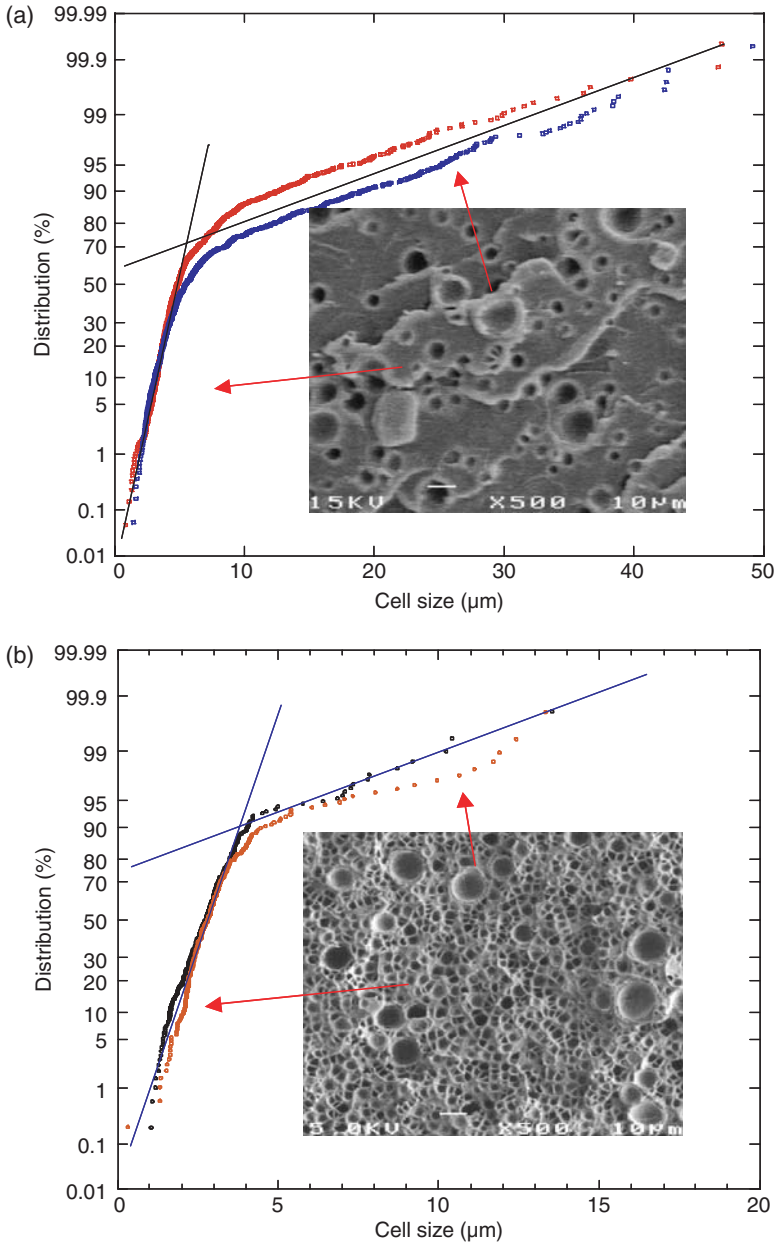
Figure 1. Cell size distribution and cellular morphology for: (a) MCF-0.9 and (b) MCF-0.7. Data for two specimens in each case are indicated.

Tensile testing was performed. Typical tensile curves of each material are shown in Figure 2. Young's modulus, UTS, and strain at break were calculated from these curves. The results are shown numerically in Table 1 and graphically in terms of relative values of density, modulus, and UTS in Figure 3. These tensile properties varied significantly upon the materials tested; Young's modulus is not lower at a relative density of 0.9 but significantly lower at a relative density of 0.7; UTS decreases with relative density; and strain at break increases significantly at a relative density of 0.9 but decreases with respect to uPC at a relative density of 0.7. In general, it appears that the area under the tensile curve, often used as a toughness indicator, is, in comparison to uPC, twice as high for MCF-0.9 and almost twice as low for MCF-0.7.

Fracture testing was performed by successive loading of the CT specimens. Individual loading led to crack propagation, which was determined from the SEM observations. An example of the fractographic
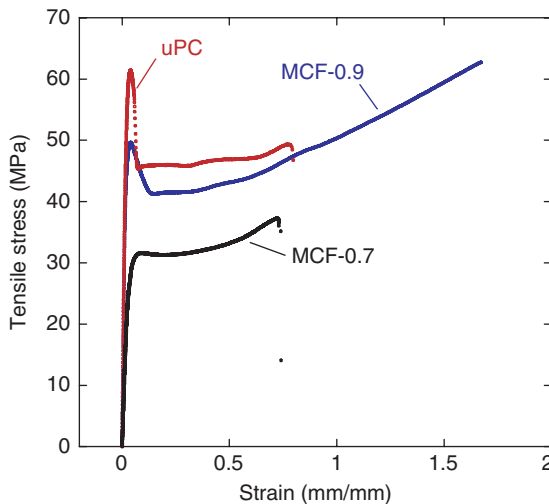

Figure 2. Tensile curve example for uPC, MCF-0.9, and MCF-0.7.

Table 1. Tensile results of the materials tested (standard deviations are indicated).

Materials	ν	E (GPa)	UTS (MPa)	ε_b (mm/mm)
UPC	0.23 ± 0.03	3.9 ± 0.2	61 ± 0.2	0.80 ± 0.05
MCF-0.9	0.26 ± 0.04	3.9 ± 0.2	50 ± 0.1	1.5 ± 0.2
MCF-0.7	0.20 ± 0.03	1.3 ± 0.2	32 ± 0.6	0.57 ± 0.20

aspect of crack propagation after six successive loadings is shown in Figure 4. From load–COD curves and crack propagation measurements, calculations of critical stress intensity factor and elastic fracture energy could be made using Equations (1) and (2). They are listed in Table 2. These toughness values show different trends, depending on which is considered. On a stress intensity basis, fracture toughness of MCF-0.9 is not significantly different from that of uPC, whereas fracture toughness of MCF-0.7 is 37% below that of uPC, thus more or less proportional to its relative density. On an energy basis, however,
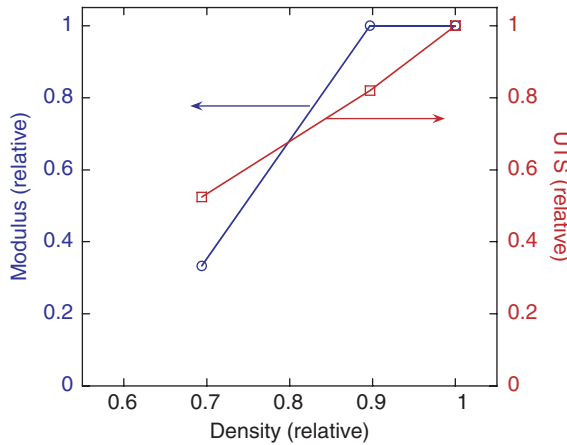

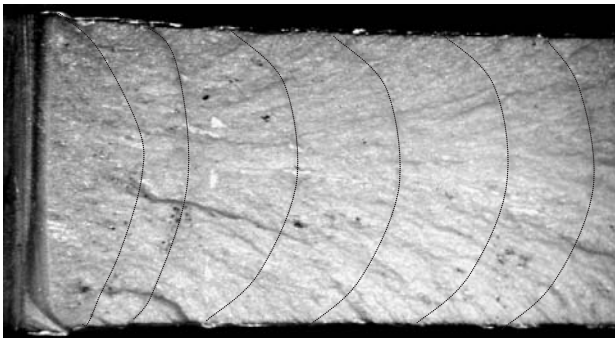**Figure 3.** Relative modulus and UTS as a function of relative density.

Figure 4. Scanning electron micrographs of the fracture surface of MCF-0.7 showing corresponding six successive crack propagation (dotted lines show curved crack fronts).

Table 2. Critical stress intensity factors and elastic fracture energies
of the materials tested (standard deviations are indicated).

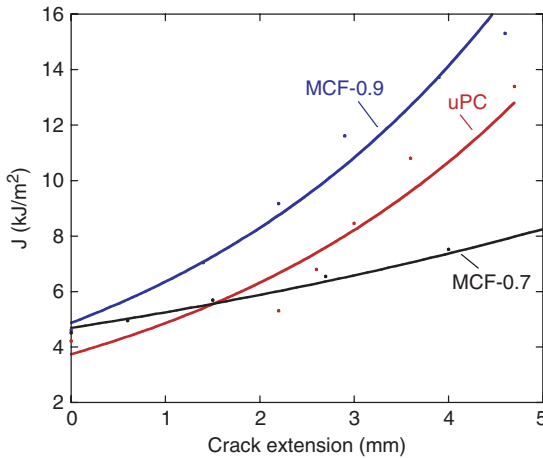| Materials	K_c (MPa$\sqrt{m}$)	J_{el} (kJ/m^2)
uPC	4.1 ± 0.4	4.1 ± 0.7
MCF-0.9	4.3 ± 0.3	4.7 ± 0.6
MCF-0.7	2.6 ± 0.1	4.6 ± 0.4

Figure 5. Toughness–propagation curves obtained.

fracture toughness of MCF-0.9 and MCF-0.7 are approximately the same, i.e., 12-15% above that of uPC.

The toughness–propagation curves, or J–R curves, were obtained from load–COD curves and crack propagation measurements using Equation (3). These curves, shown in Figure 5, indicate that all materials tested have stable crack propagation, i.e., additional crack extension could be obtained only if an additional fracture energy was provided; unstable crack propagation or brittle fracture was not observed. They also show that MCF-0.9 and uPC have parallel fracture curves, suggesting that difference in their toughness at the onset of fracture remains throughout the crack propagation. Toughness–propagation curve of MCF-0.7 had a curve with a considerably smaller slope, i.e., the amount of additional energy required for further propagation was lower than that for uPC and MCF-0.9. After close to 2 mm of propagation, crack propagation resistance of MCF-0.7 became lower than that of uPC.
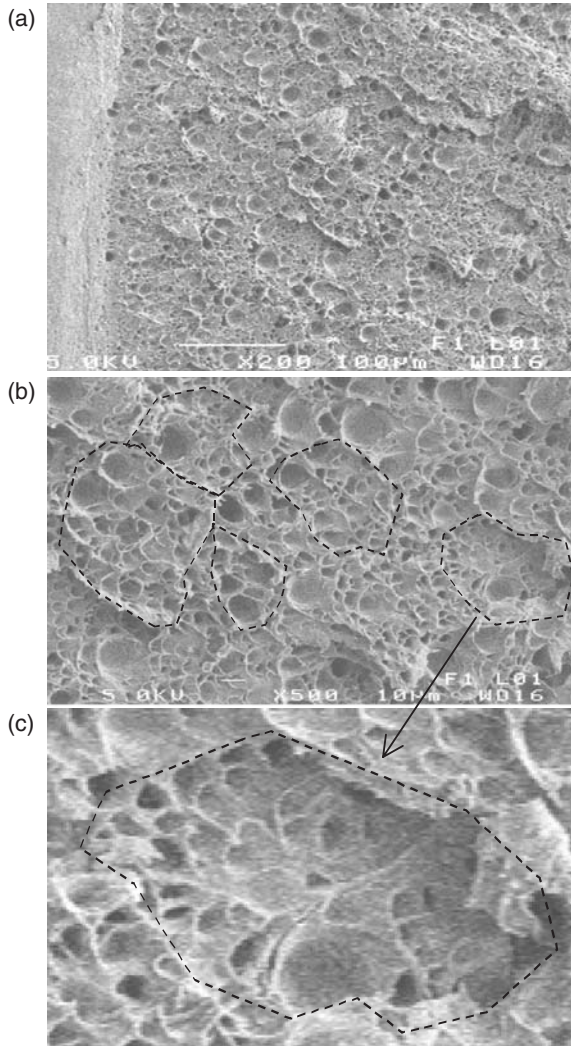
Figure 6. Fractographs of MCF-0.7 at: (a) low; (b) medium; and (c) high magnifications showing fracture by coalescence of large voids formed at larger cells (some highlighted by dotted lines), containing smaller voids formed at smaller cells. Crack propagation direction is from left to right.

Fracture surface observations were made to understand how fracture occurred in MCF-0.9 and MCF-0.7. Fractographs are shown for MCF-0.7 at three levels of magnification in Figure 6. These observations reveal that fracture occurs in MCFs by the formation of voids by shear yielding
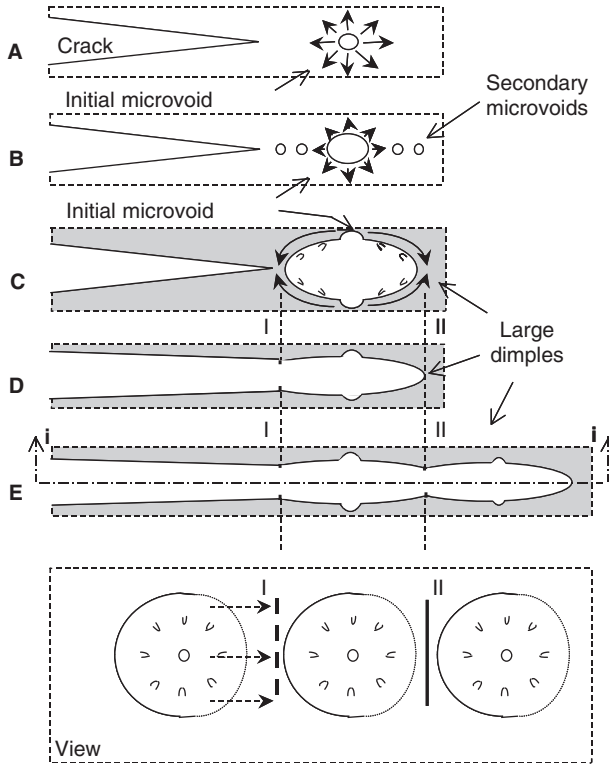
Figure 7. Schematic representation of the discontinuous crack propagation process observed in the MCFs in 5 steps (A: void initiation, B: secondary initiation and growth, C: void coalescence, D: dimple coalescence, E: return to A–D). (From Journal of Materials Science Letters, vol. 20, 2001, 1901–1904, Bureau, M.N. Denault, J. and Dickson, J.I. Figure 2(a). With kind permission of Springer Science and Business Media).

at cells acting as stress concentrators in front of the crack due to stress triaxiality. These voids form first at larger cells because of their associated higher stress concentration factor. As the stress increases, these voids grow in size, reach smaller cells in their vicinity, and coalesce with the latter to form large voids or *dimples*. At a certain point, these large dimples form along the crack front merge and macroscopic crack propagation occurs. Since unstable crack propagation is not observed, this sequence of events continues upon loading, which gives rise to a discontinuous crack propagation process quite similar to that observed in immiscible polymer blends [12]. This discontinuous crack propagation is schematically represented in Figure 7.

DISCUSSION

From the fracture toughness and fractographic observations, it appears that the fracture toughness of PC-based MCFs can be as high as and even greater than the fracture toughness of uPC, provided that they have the appropriate cellular structure. In the present case, void formation in MCFs occurred at larger cells, at stresses lower than those in uPC, as indicated by the tensile curves in Figure 2. However, fracture toughness results show that the onset of crack propagation occurred at higher *J*-values in MCFs than in uPC. Fractographic observations show that this growth stage occurred by shear yielding and coalescence with smaller voids in the vicinity of first larger void. Since fracture is the result of initiation, growth, and coalescence of defects (voids in MCFs and shear bands in uPC), the growth and coalescence stages in MCFs must be slower to account for their higher toughness. Thus it must be concluded that the bi-modal distribution of the MCFs studied provides an appropriate balance between large cells, which initiate voids, and smaller cells, which control growth, to obtain high fracture energy absorption before the crack propagation occurs (i.e., fracture toughness).

CONCLUSIONS

The PC-based MCFs presented a bi-modal distribution of cells with median cell sizes of 3–4 and 6–9 μm for both cell populations. Their tensile properties were generally lower than those of uPC, more or less proportionally to their relative density, which indicated that the cells therein acted as stress initiation sites. Fracture results showed that crack propagation, by growth and coalescence of voids, occurred at higher fracture toughness in MCFs than in uPC. The bi-modal distribution of MCFs provided the balance between large cells, which initiate voids, and smaller cells, which control growth, to obtain high fracture toughness.

ACKNOWLEDGMENTS

REFERENCES

1. Martini, J.E., Suh, N.P. and Waldman, F.A. (1984). US Patent No. 4,473,665.
2. Kumar, V. and Suh, N.P. (1990). *Polym. Eng. Sci.*, **30**: 1323–1329.
3. Barlow, C.C., Weller, J.E., Kumar, V., Bordia, R.K. and Flinn, B. (1998). *Proc. ASME on Porous, Cellular and Microcellular Materials*, MD-82, 45–51.
4. Collias, D.I., Baird, D.G. and Borggreve, R.J.M. (1994). *Polymer*, **35**: 3978–3983.
5. Collias, D.I. and Baird, D.G. (1995). *Polym. Eng. Sci.*, **35**: 1178–1183.
6. Kumar, V., VanderWel, M., Weller, J. and Seeler, K.A. (1994). *J. Eng. Mater. Techn.*, **116**: 439–445.
7. Kumar, V., Weller, J.E. and Murray, R. (1995). *ANTEC 1995*, SPE, 2202–2206.
8. Wing, G., Pasricha, A., Tuttle, M. and Kumar, V. (1995). *Polym. Eng. Sci.*, **35**: 673–679.
9. Gibson, L.J. and Ashby, M.F. (1997). *Cellular Solids: Structure and Properties*, **2nd edn**, Cambridge University Press, Cambridge, UK, p. 510.
10. ASTM D256-02 Standard Test Methods for Determining the Izod Pendulum Impact Resistance of Plastics.
11. ASTM D6110-02 Standard Test Methods for Determining the Charpy Impact Resistance of Notched Specimens of Plastics.
12. Bureau, M.N., Denault J. and Dickson, J.I. (2001). *J. Mater. Sci. Lett.*, **20**: 1901–1904.